JOURNAL OF MATERIALS SCIENCE **36** (2001) 4893–4902

Particle size dependence of fatigue crack propagation in SiC particulate-reinforced aluminium alloy composites

Z. Z. CHEN
Gifu University, 1-1 Yanagido, Gifu 501-1193, Japan

K. TOKAJI
Department of Mechanical and Systems Engineering, Faculty of Engineering, Gifu University, 1-1 Yanagido, Gifu 501-1193, Japan
E-mail: tokaji@mech.gifu-u.ac.jp

A. MINAGI
Department of Mechanical Engineering, Osaka Prefectural College of Technology, 26-12 Saiwai-cho, Neyagawa 572-8572, Japan

Fatigue crack propagation (FCP) and fracture mechanisms have been studied for two orientations in powder metallurgy 2024 aluminium alloy matrix composites reinforced with three different sizes of silicon carbide particles. Particular attention has been paid to make a better understanding for the mechanistic role of particle size. The FCP rates of the composites decreased with increasing particle size regardless of orientation and were slightly faster in the FCP direction parallel to the extrusion direction. After allowing for crack closure, the differences in FCP rate among the composites and between two orientations were significantly diminished, but the composites showed lower FCP rates than the corresponding unreinforced alloy. Fracture surface roughness was found to be more remarkable with increasing particle size and in the FCP direction perpendicular to the extrusion direction. Taking into account the difference in the modulus of elasticity in addition to crack closure, the differences in FCP rate between the unreinforced alloy and the composites were almost eliminated.

1. Introduction

Metal matrix composites reinforced with discontinuous phases in the forms of short fiber, whisker, and particulate essentially exhibit a considerably enhanced strength and stiffness compared with the corresponding unreinforced alloys. Among those discontinuously reinforced materials, aluminium-based metal matrix composites reinforced with silicon carbide particulates (SiC_p/Al) are particularly attractive since the conventional metallurgical and machining processing techniques, such as direct casting, powder metallurgy, rolling, forging, and extrusion can be applied for their fabrication. Although the second phase additions can cause reduced tensile ductility, lower fracture toughness, and in some cases, decreased fatigue resistance compared with the constituent matrix alloy, SiC_p/Al composites still have potential in structural applications because of considerable weight saving due to their specific properties.

Since fatigue properties are critical for load bearing applications, a number of studies have been reported so far. In SiC_p/Al composite systems, there are several microstructural parameters such as volume fraction, distribution and size of SiC particles, interface properties, and matrix properties, each of which may exert a significant influence on the fatigue properties. The volume fraction of particles is one of the most important variables in determining the fatigue properties, thus many previous works have been concentrated on this issue. Particle size is assumed to be another key factor for a given volume fraction and matrix property, but only a few studies concerning the effect of particle size on fatigue strength have been reported. Hall *et al*. [1] showed that fatigue life increased as particle size decreased. The present authors [2] also indicated that fatigue strength increased in the composite with fine particle size, but decreased with increasing particle size, compared with the unreinforced alloy. In the composites with coarse particle sizes, fatigue cracks were initiated at or near the particle/matrix interface and then cracks tended to grow along the interface, leading to the decreased fatigue strength. Fatigue crack propagation (FCP) is another important property for engineering applications, thus the purpose of the present study is to develop a better understanding for the effect of particle size on FCP behaviour and fracture mechanisms, because the role of particle size in the propagation stage of large cracks is expected to differ from that observed in crack initiation and subsequent small crack growth.

There have been many FCP studies in SiC_p/Al composite systems, in which the role of microstructural variables such as volume fraction of particles [3, 4], matrix property [5–9], particle distribution [10, 11] and orientation [6, 9] was discussed, but very limited studies on the effect of particle size have been reported. Shang *et al.* [12] examined the FCP behaviour in SiC_p/MB78 composites with two different particle sizes and showed that FCP rates in the fine-SiC composite are faster, and threshold stress intensity was lower, compared with the coarse-SiC composite. Li and Misawa [13] found a considerable influence of particle size on FCP behaviour in SiC_p/6061Al composites and indicated that the effect of particle size disappeared after allowing for crack closure.

In the present work, FCP behaviour was studied in SiC_p/2024Al composites with three different particle sizes for a given volume fraction of the reinforcement, and the effect of particle size and fracture mechanisms were discussed on the basis of crack closure measurement, crack path and fracture surface observation. In addition, the effect of orientation on FCP behaviour was also discussed.

2. Experimental details

2.1. Material and microstructure

Aluminium alloy 2024 fabricated by powder metallurgy was used in the unreinforced condition and with 10 wt% SiC_p reinforcement. The chemical composition (wt%) is; Si 0.13, Fe 0.24, Cu 4.57, Mn 0.63, Mg 1.65, Cr 0.01, Zn 0.091, Ti 0.02, balance Al. Gas atomized powders of 2024 alloy were blended with SiC particles, cold compacted and then degassed at 450°C. The same processing procedure was employed for the unreinforced alloy. Extrusion at 430°C was used to produce bars with a diameter of 35 mm. Three different nominal particle sizes of 5, 20 and 60 μm were evaluated. Hereafter, each composite is denoted as 5 μm SiC_p, 20 μm SiC_p, and 60 μm SiC_p.

Fig. 1 shows the microstructures of the sections perpendicular (R-plane) and parallel (L-plane) to the extrusion direction in the unreinforced alloy and the composites. It can be seen that SiC particles tend to be weakly aligned in the extrusion direction. Microstructural parameters measured on the both planes are listed in Table I. Particle size which was obtained as the average

TABLE I Quantitative analysis of microstructural parameters in SiC_p/Al composites

Alloy	Plane	Particle size (μm)	Interparticle spacing (μm)	Area fraction of particle (%)
5 μm SiC_p	R	3.2	11.1	10.8
	L	3.3	9.8	10.9
20 μm SiC_p	R	11.6	39.4	10.4
	L	14.0	39.8	11.2
60 μm SiC_p	R	37.7	113.9	12.1
	L	41.7	109.5	11.9

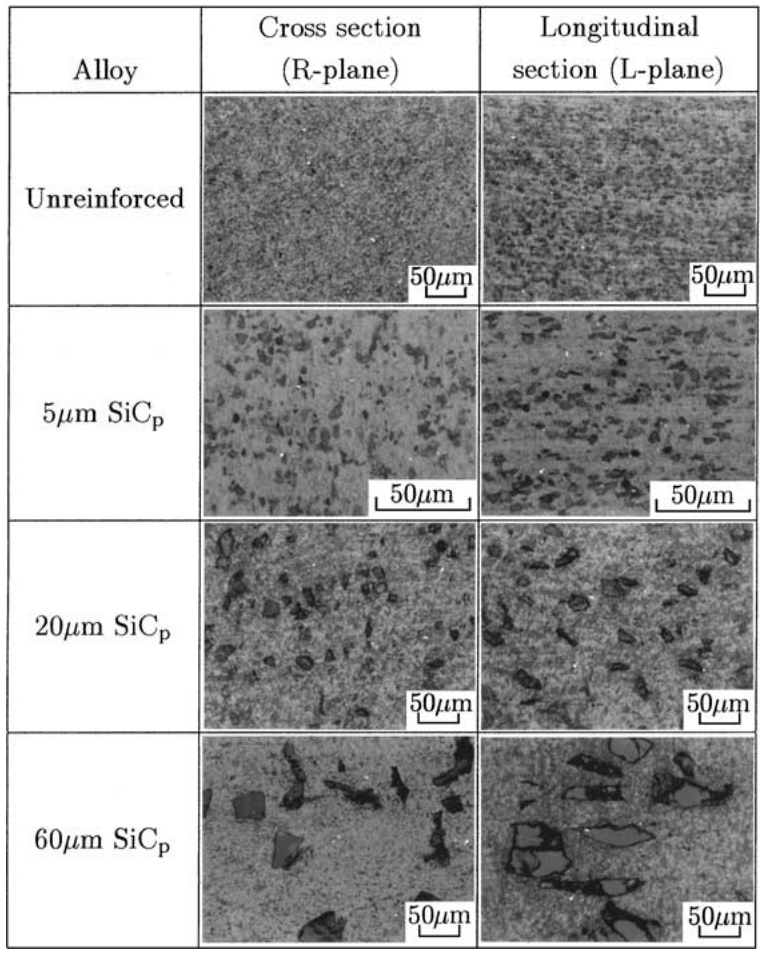

Figure 1 Microstructures of unreinforced alloy and SiC_p/Al composites. Note that the magnification of micrographs for the 5 μm SiC_p/Al composite differs from that for the unreinforced alloy and other composites.

diameter of circles having equivalent area and area fraction of particles were measured on an image analysis system and interparticle spacing was measured manually from photomicrographs. As can be seen in the table, the average particle sizes are smaller than the nominal particle sizes in all the composites and are slightly larger in L-plane than in R-plane because of the aspect ratio of particles of approximately 1.7. As expected, the interparticle spacing increases with increasing particle size, but no differences were seen between both planes. The area fraction of particles ranges from 10.4 to 12.1% regardless of particle size and plane.

2.2. Specimen preparation

Tensile specimens with a diameter of 8 mm and CT specimens with a width of 24 mm and a thickness of 5 mm were machined from the as-received bars. CT specimens with two different orientations were prepared, i.e. R-L and L-R orientations, where R and L represent the directions perpendicular and parallel to the extrusion directions, respectively. Specimens were solution treated at 495°C for 1h, quenched in water and then aged at 190°C to achieve peak-aged condition. With increasing particle size, the artificial ageing time was decreased and the Vickers hardness increased, which were 5 h and 129 for the unreinforced alloy, 5 h and 135 for the 5 μm SiC_p composite, 3 h and 137 for the 20 μm SiC_p composite, and 2.5 h and 144 for the 60 μm SiC_p composite, respectively.

2.3. Mechanical properties

Tensile properties of the unreinforced alloy and the composites studied are listed in Table II. Proof stress is slightly decreased with the addition of SiC particles and a little effect of particle size can be seen. For all but the largest particle size, the presence of SiC particles increases tensile strength. Compared with the unreinforced alloy, the elongation and reduction of area of all the composites significantly decrease, but the particle size dependence cannot be seen. The modulus of elasticity is almost the same for all the composites and there is a 17% increase compared with the unreinforced alloy.

2.4. Procedures

Experiments were conducted on an electro servohydraulic fatigue testing machine operating at a frequency of 10 Hz in laboratory air at ambient temperature. Increasing and decreasing stress intensity factor range, ΔK, tests were performed at a fixed stress ratio, R, of 0.05. For the latter tests, load shedding techniques with a load reduction of 5% were employed. Prior to experiment, a fatigue precrack of approximately 2 mm in length from the notch root was introduced under a decreasing ΔK condition. Crack length was monitored by a travelling microscope with a resolution of 10 μm and crack closure was measured by a compliance method using a strain gauge mounted on the back face of the CT specimen.

Crack path profiles and fracture surfaces were examined in detail using an optical microscope and scanning electron microscope (SEM), respectively.

TABLE II Mechanical properties of unreinforced alloy and SiC_p/Al composites

Alloy	Proof stress ($\sigma_{0.2}$) (MPa)	Tensile strength (σ_B) (MPa)	Elongation (ϕ) (%)	Reduction of area (ψ) (%)	Elastic modulus (E) (GPa)
Unreinforced	373	454	9	26	61
5 μm SiC_p	365	462	5	8	71
20 μm SiC_p	357	479	6	10	70
60 μm SiC_p	356	452	4	8	72

3. Results and discussion

3.1. Relationships between FCP rate, da/dN, and ΔK

Fig. 2 shows the relationships between da/dN and ΔK, where Fig. 2a and b represent the data for L-R and R-L orientations, respectively. As can be seen in the figures, above approximately $da/dN = 5 \times 10^{-6}$ mm cycle^{-1} the da/dN-ΔK relationships for the unreinforced alloy and all the composites can be expressed by the Paris law.

For L-R orientation (Fig. 2a), the 5 μm SiC_p composite shows the fastest FCP rates in the entire ΔK region tested, while the FCP rates of the 20 μm SiC_p and 60 μm SiC_p composites and the unreinforced alloy are nearly the same in intermediate and high ΔK regions, but the 60 μm SiC_p composite exhibits the highest FCP resistance in low ΔK region. Also included in the figure are the data of the unreinforced alloy without heat treatment (solid symbol) and the FCP rates are slightly faster than, or almost the same as, those of the 5 μm SiC_p composite. It is thought that the difference in FCP behaviour between the unreinforced alloys with and without heat treatment is probably attributed to the effect of residual stress, as will be discussed later.

The effect of particle size is rather small in R-L orientation (Fig. 2b). However, the FCP rates of the 5 μm SiC_p and 20 μm SiC_p composites are identical, but the 60 μm SiC_p composite appears to show slightly lower FCP rates compared with those composites in the entire ΔK region. The unreinforced alloy exhibits the lowest FCP rates in intermediate ΔK region, while the fastest in low ΔK region. From the comparison of Fig. 2a and b, the FCP rates of R-L orientation are slightly faster than those of L-R orientation in all the materials.

It is summarized from Fig. 2 that the FCP resistance of the SiC_p/Al composites tends to increase with increasing particle size regardless of orientation. However, the FCP behaviour of the unreinforced alloy makes difficult to understand the effect of the addition of SiC particles. Macroscopic examination of fracture surfaces revealed a very large curvature of the crack front in the unreinforced alloy compared with the composites, i.e. the crack front considerably advanced at the midthickness. This may suggest the existence of significantly large compressive residual stresses at or near the specimen surfaces.

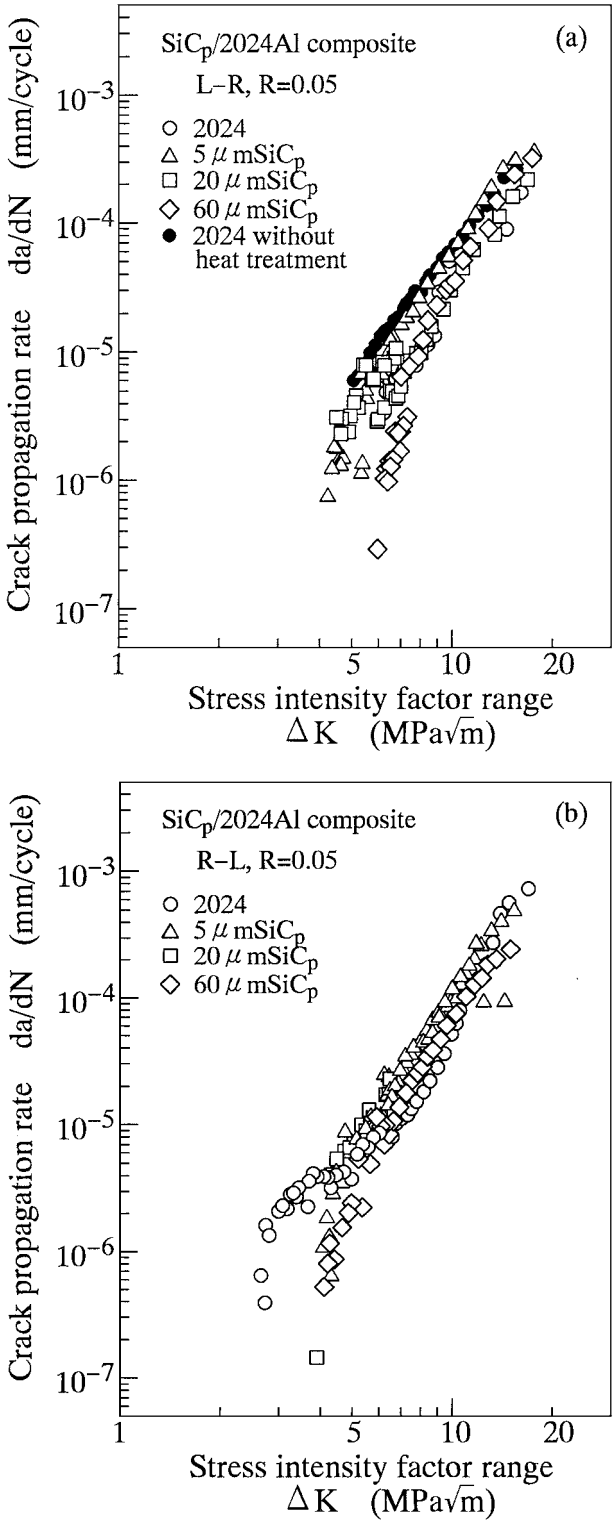

Figure 2 Relationships between crack propagation rate and stress intensity factor range: (a) L-R orientation, (b) R-L orientation.

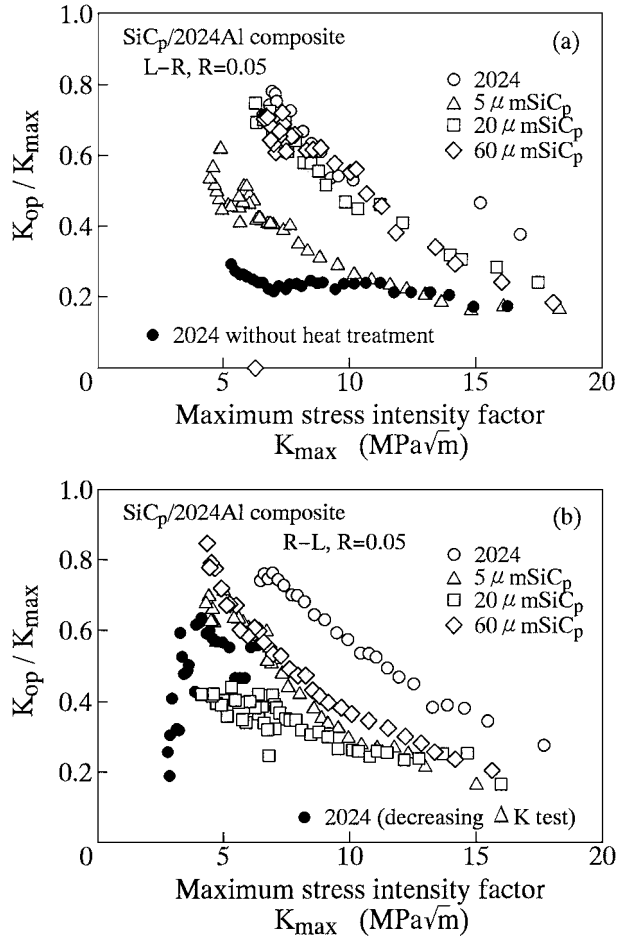

Figure 3 Crack closure behaviour: (a) L-R orientation, (b) R-L orientation.

3.2. Crack closure behaviour

Crack closure behaviour, K_{op}/K_{max}, is shown in Fig. 3 as a function of K_{max}, where K_{op} and K_{max} are the crack opening and maximum stress intensity factors, respectively. The data for all the materials exhibit the same general form, showing increasing closure level with decreasing K_{max}. For L-R orientation (Fig. 3a), the closure levels of the 20 μm SiC_p and 60 μm SiC_p composites are almost the same and attain to extremely high value in low K_{max} region and the 5 μm SiC_p composite shows lower closure levels in the entire K_{max} region. Remarkable crack closure is obtained for the unreinforced alloy [3, 12], which is almost comparable to that of the 20 μm SiC_p and 60 μm SiC_p composites. On the contrary, it should be noted that the unreinforced alloy without heat treatment represents very low closure levels. This seems to give another evidence of the existence of compressive residual stresses in the unreinforced alloy, which causes remarkable crack closure.

A slightly different behaviour can be seen for R-L orientation (Fig. 3b), where the lowest closure levels are obtained in the 20 μm SiC_p composite and the 5 μm SiC_p and 60 μm SiC_p composites exhibit the same closure levels. In the unreinforced alloy, the crack closure behaviour is found to depend strongly on the types of FCP experiments. Under increasing ΔK condition (open symbol), the closure levels are extremely high and increase with decreasing K_{max}, as well as for L-R orientation. However, under decreasing ΔK condition (solid symbol), the closure levels decrease with decreasing K_{max}. Fig. 4 represents the crack closure behaviour under both test conditions as a function of crack length. This result also provides further evidence showing the effect of compressive residual stress in the unreinforced alloy. Under decreasing ΔK condition, the closure levels decrease with increasing crack length in spite of the decrease in ΔK. This indicates that the decrease in closure level due to the release of compressive residual stress with increasing crack length takes

place more rapidly than the increase with decreasing ΔK. However, further study is needed to make clear the reason why such large compressive residual stress was introduced.

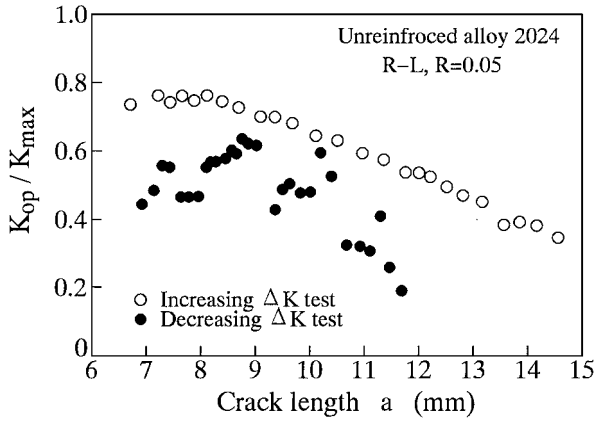

Figure 4 Crack closure behaviour in unreinforced alloy as a function of crack length.

3.3. Fracture surface morphology

The crack paths of the unreinforced alloy were rather smooth regardless of ΔK and orientation. This clearly indicates that the remarkable crack closure seen in Fig. 3 cannot be attributed to fracture surface roughness. Fig. 5 reveals crack path profiles at two different ΔK values in all the composites. Tortuous crack paths can be seen, which becomes more remarkable with increasing particle size, because there is a strong propensity that cracks grow avoiding particles, as will be described later. Crack paths are also more tortuous for L-R orientation compared with R-L orientation. This results from the alignment of SiC particles to the extrusion direction (L-plane) (see Fig. 1) and the aspect ratio of particles.

Representative examples of the fracture surface morphology are shown in Fig. 6, which were obtained at the midthickness of the specimens at $\Delta K = 6\ \mathrm{MPa}\sqrt{\mathrm{m}}$ in all the composites. As described above, two particular points are clearly noticed: one is increasing surface roughness with increasing particle size and the other

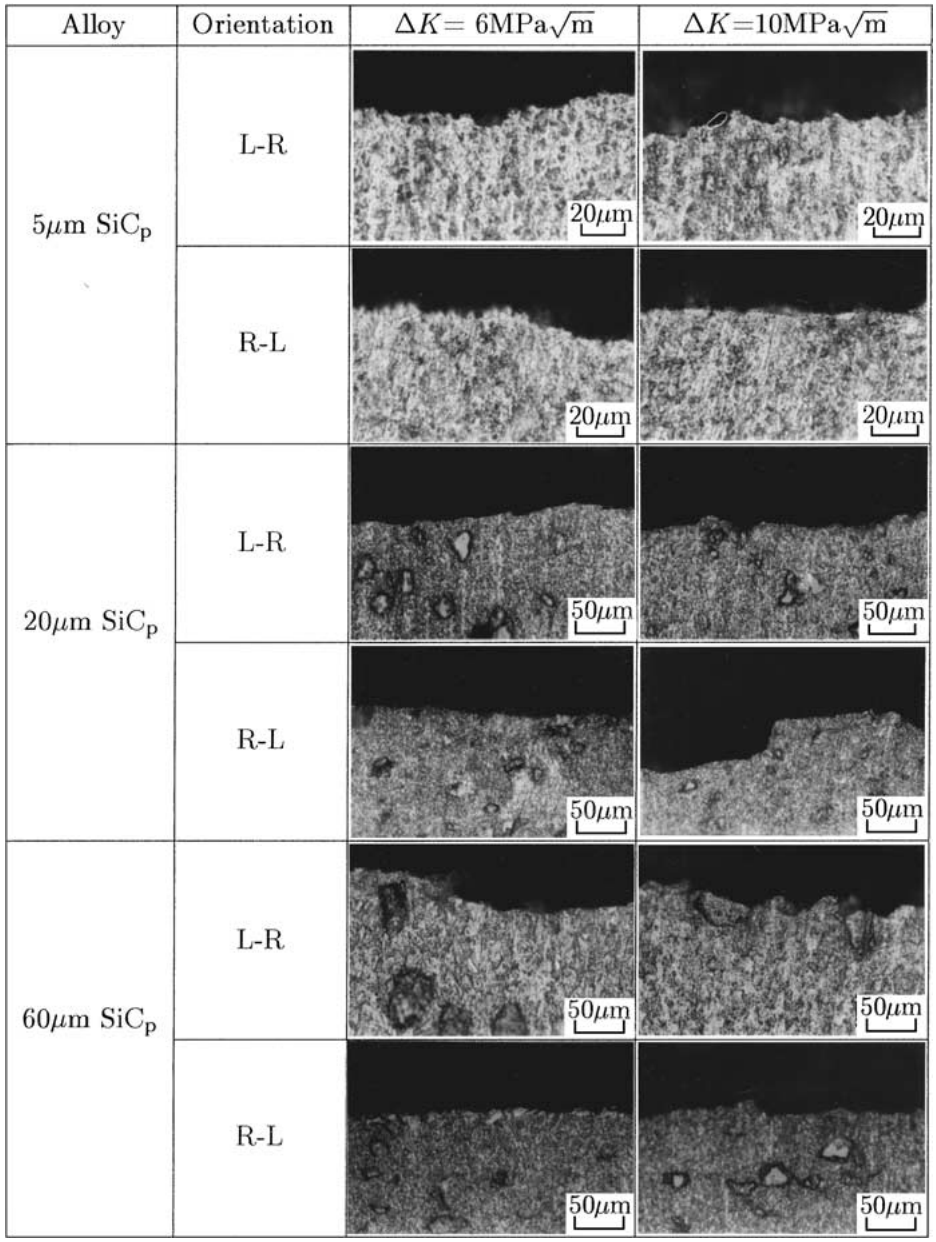

Figure 5 Optical micrographs showing crack path profiles in SiC_p/Al composites. Note that the magnification of micrographs for the 5 μm SiC_p/Al composite differs from that for other composites.

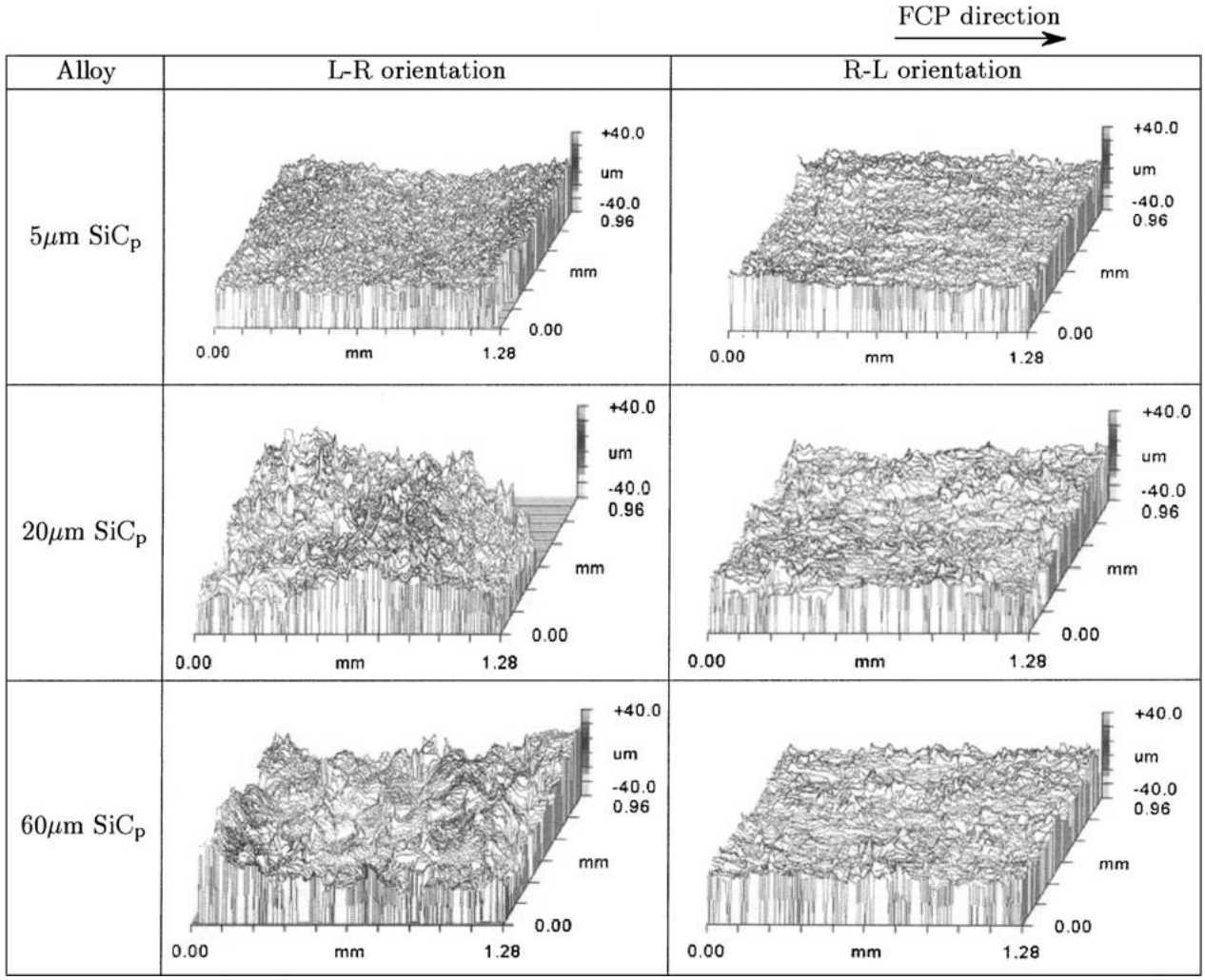

Figure 6 Fracture surface roughness observed at $\Delta K = 6$ MPa$\sqrt{\text{m}}$ in SiC_p/Al composites.

is much rougher surface for L-R orientation than for R-L orientation. Although there is an exception that crack closure behaviour does not correspond to fracture surface roughness (remarkable crack closure, but low roughness for R-L orientation in the 5 μm SiC_p composite), crack closure of the present SiC_p/Al composites is assumed to be mainly induced by fracture surface roughness resulting from crack path deflection.

3.4. Particle size dependence of intrinsic FCP resistance in the composites

The FCP behaviour characterized in terms of the effective stress intensity factor range, ΔK_{eff}, is represented in Fig. 7. It should be noticed that the FCP rates of all the composites after allowing for crack closure are nearly the same regardless of orientation, i.e. the differences in FCP rate among the composites seen in Fig. 2 are almost diminished, indicating that crack closure is responsible for the particle size dependence of FCP behaviour. It has also been indicated that with the closure effects accounted for, the effects of volume fraction and particle size were significantly diminished or eliminated [3, 13]. Also noticed in the figures is the superior intrinsic FCP resistance of the composites to the unreinforced alloy. From the comparison of L-R (Fig. 7a) and R-L (Fig. 7b) orientations, the FCP behaviour for both orientations is almost identical, with the exception of a slight difference in high ΔK_{eff} region, showing that crack closure is also responsible for the effect of orientation. Therefore, it is concluded that the intrinsic FCP resistance of the composites does not depend on particle size and orientation.

3.5. FCP mechanisms of the composites

Figs 8–10 reveal SEM micrographs of the fracture surfaces at two different ΔK values in all the composites. In the 5 μm SiC_p composite (Fig. 8), there is no remarkable difference in fracture surface appearance between both orientations and no SiC particles can be seen even in high ΔK region where the reversed plastic zone size becomes large, indicating that the crack grow predominantly within the matrix. This also suggests that the particle/matrix interface is strong enough to inhibit interfacial cracking. Although the crack grows avoiding particles, the resulting fracture surface roughness is relatively small (see Fig. 6) because of the fine particle size.

The features of fracture surface appearance are very similar between the 20 μm SiC_p and 60 μm SiC_p composites (Figs 9 and 10). Regardless of orientation, some

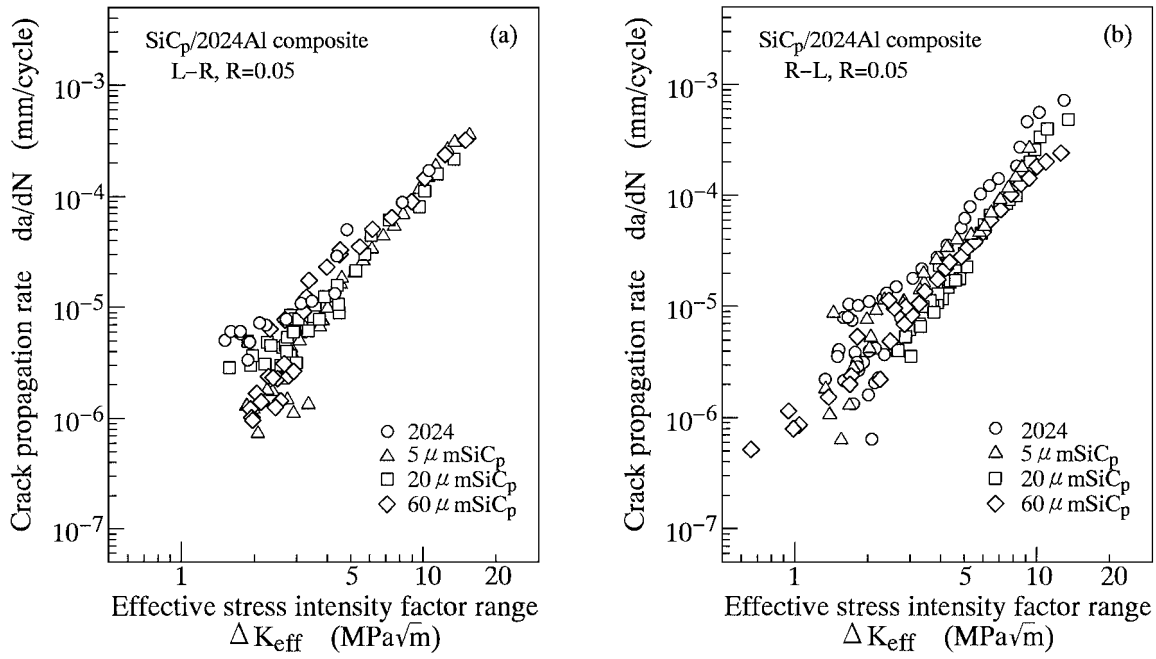

Figure 7 Relationships between crack propagation rate and effective stress intensity factor range: (a) L-R orientation, (b) R-L orientation.

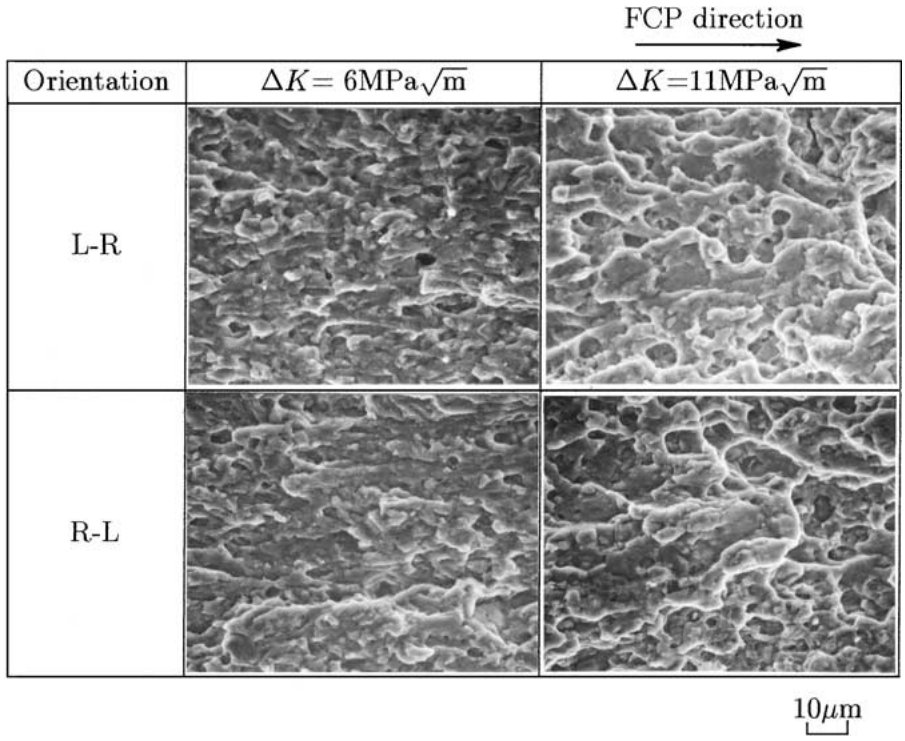

Figure 8 SEM micrographs of fracture surfaces in 5 μm SiC_p/Al composite.

particles can be seen on the fracture surfaces and the number of particles tends to increase with increasing ΔK. It should be noted that most of particles appearing on the fracture surfaces are fractured. If particles are located ahead of the crack tip, then particle fracture would occur; this propensity would be marked in the composites with coarser particles because the particle strength decreases with increasing particle size [1]. In addition, no interfacial crackings or voids around particles are seen independent of ΔK, also suggesting the strong interfacial strength.

Fig. 11 shows the area fraction of particles appearing on the fracture surfaces in the 20 μm SiC_p and 60 μm SiC_p composites as a function of ΔK. As already described, no particles were seen in the 5 μm SiC_p composite regardless of ΔK. With the exception of larger fractions in the 60 μm SiC_p composite than the 20 μm SiC_p composite over the ΔK range examined, both composites exhibit the same tendency. Three particular points are noticed; the first point is the increased fraction of particles with increasing ΔK [3], but the fractions of particles at all ΔK values are

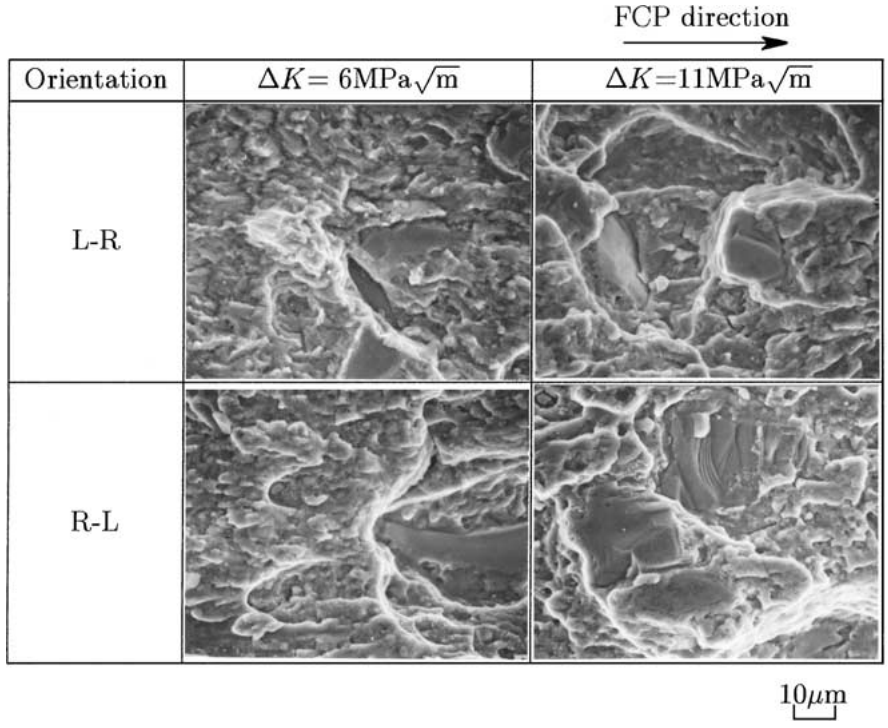

Figure 9 SEM micrographs of fracture surfaces in 20 μm SiC_p/Al composite.

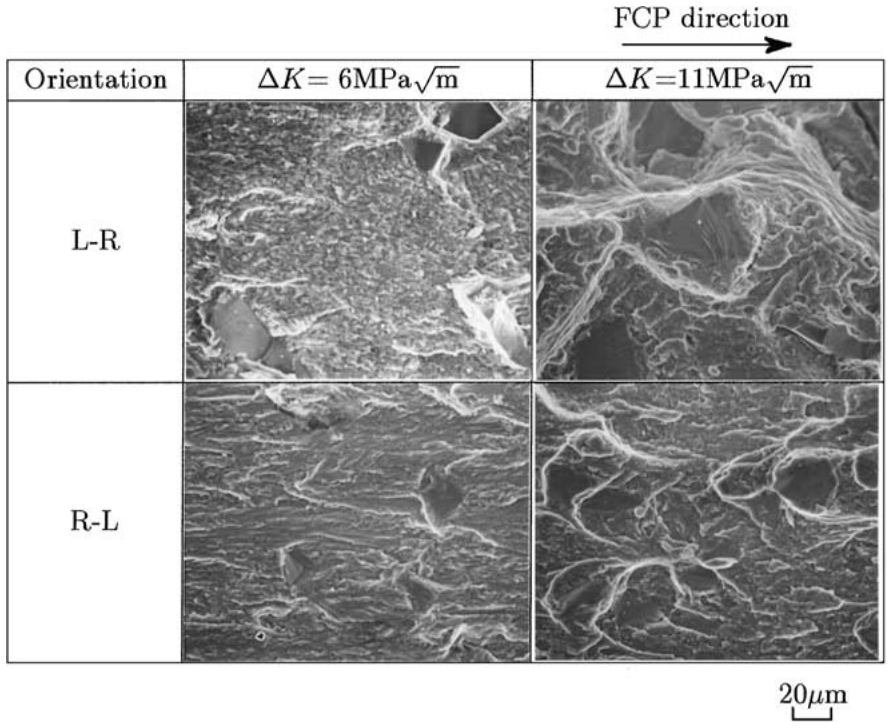

Figure 10 SEM micrographs of fracture surfaces in 60 μm SiC_p/Al composite.

smaller than those examined on the metallographic section. This suggests that cracks tend to avoid particles even in high ΔK region. The second point is the larger fraction of particles for R-L orientation than for L-R orientation, resulting from larger area of each particle due to the aspect ratio and the number of particles in the former orientation. The third point is nearly the same fraction of particles in a pair of fracture surfaces. This results from the fact that most of particles appearing on the fracture surfaces were fractured as seen in Figs 9 and 10.

3.6. Correlation of FCP data with ΔK normalized by the modulus of elasticity

It has been well known that FCP rates are strongly dependent on the modulus of elasticity, E. FCP rates of materials with smaller E are generally faster than those of materials with larger E, but when FCP data are characterized by ΔK normalized with respect to E, $\Delta K/E$, differences in FCP response tend to be largely diminished. Such a result was also obtained in SiC_p/6061Al composite [11], in which crack closure measurement has not been done. As shown in Table II, the particle

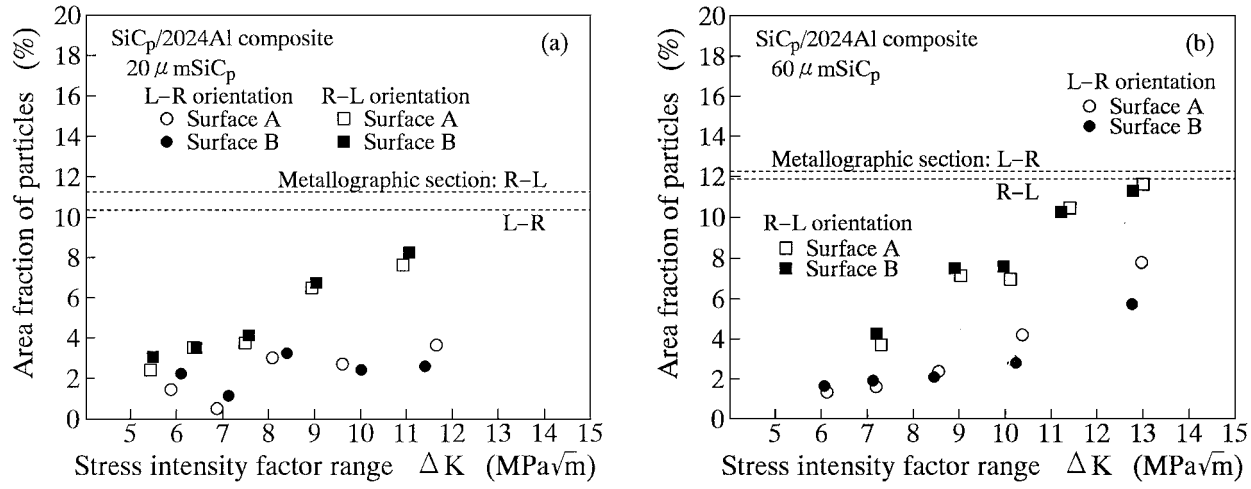

Figure 11 Area fraction of SiC particles appearing on fracture surfaces as a function of stress intensity factor range: (a) 20 μm SiC_p/Al composite, (b) 60 μm SiC_p/Al composite.

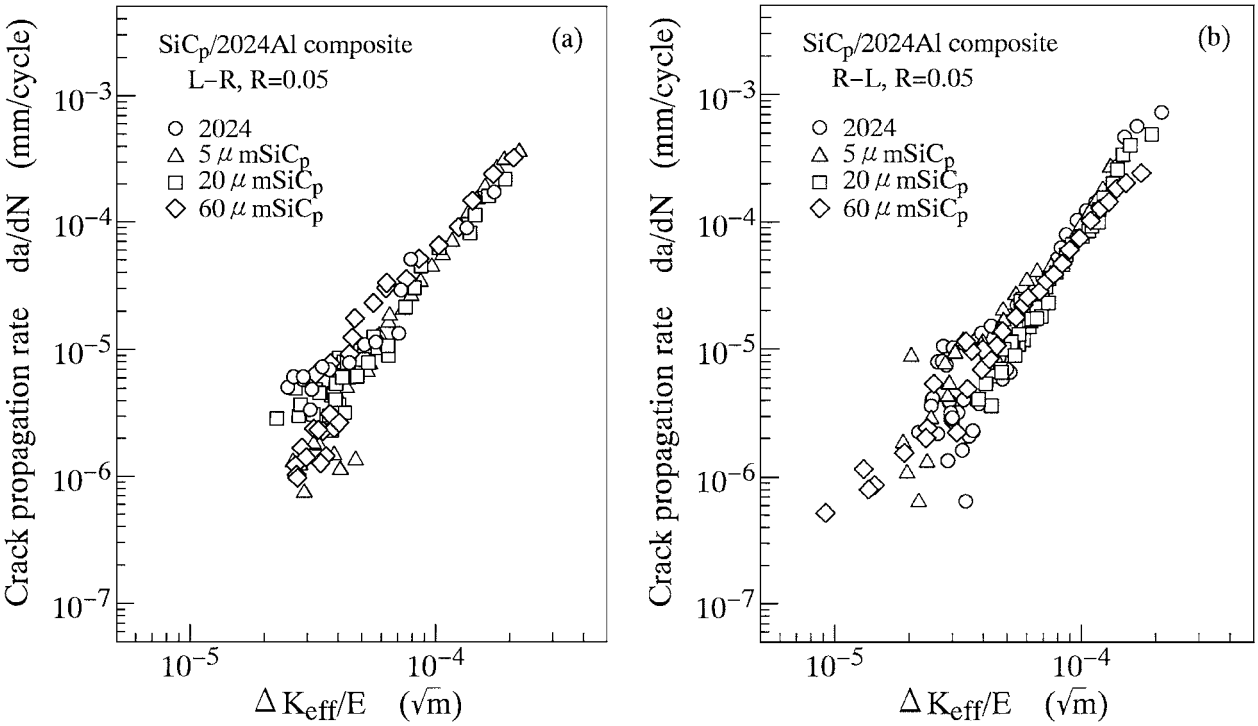

Figure 12 Relationships between crack propagation rate and effective stress intensity factor range normalized with respect to elastic modulus: (a) L-R orientation, (b) R-L orientation.

size exerted no significant influence on the E values of the composites which were 17% larger compared with the unreinforced alloy. Fig. 12 shows the FCP behaviour characterized in terms of $\Delta K_{\text{eff}}/E$. It can be clearly seen that the differences in FCP rate between the unreinforced alloy and the composites observed in Fig. 7 almost disappear regardless of orientation. Therefore, the intrinsic FCP resistance after taking into account crack closure and the modulus of elasticity does not depend on the addition of the reinforcement and particle size.

4. Conclusions

FCP behaviour was studied in SiC_p/2024Al composites with three different particle sizes, 5 μm, 20 μm and 60 μm, for a given volume fraction of the reinforcement, and the effects of particle size and fracture mechanisms were discussed on the basis of crack closure measurement, crack path and fracture surface observation. The effect of orientation was also discussed. The following conclusions can be made.

1. When the FCP data were characterized in terms of ΔK, FCP rates tended to decrease with increasing particle size regardless of orientation. After allowing for crack closure, the differences in FCP rate among the composites were almost diminished and the composites exhibited lower FCP rates than the unreinforced alloy.

2. In the composites, crack deflection i.e. fracture surface roughness was more remarkable with

increasing particle size and in L-R orientation, which led to significant roughness induced crack closure.

3. Taking into account the difference in the modulus of elasticity in addition to crack closure, the differences in FCP behaviour between the unreinforced alloy and the composites almost disappeared.

4. No particles were observed on the fracture surfaces even in high ΔK region in the 5 μm SiC_p composite and thus the crack propagated predominantly within the matrix in the entire ΔK region.

5. In the 20 μm SiC_p and 60 μm SiC_p composites, the area fraction of particles appearing on the fracture surfaces was the same in a pair of fracture surfaces, reflecting particle fracture. It increased with increasing ΔK and in R-L orientation, but was smaller than that examined on the metallographic sections even in high ΔK region, thus there was the strong propensity that cracks grew avoiding particles.

Acknowledgments

The authors are grateful to Sumitomo Light Metal Industries Ltd. for the provision of the material. Thanks are also due to Mr. H. Matsuhashi, Mr M. Kasuga and Mr H. Nagaya for the testing work.

References

1. J. D. HALL, J. W. JONES and A. K. SACHDEV, *Mater. Sci. Eng.* **A183** (1994) 69.
2. K. TOKAJI, H. SHIOTA and K. KOBAYASHI, *Fatigue Fract. Eng. Mater. Struct.* **22** (1999) 281.
3. Y. SUGIMURA and S. SURESH, *Metall. Trans.* **23A** (1992) 2231.
4. T. KOBAYASHI, H. IWANARI, S. HAKAMATA, M. NIINOMI and H. TODA, *J. Japan Inst. Metals* **55** (1991) 72.
5. D. L. DAVIDSON, *Engng Fract. Mech.* **33** (1989) 965.
6. W. A. LOGSDON and P. K. LIAW, *ibid.* 24 (1986) 737.
7. D. M. KNOWLES and J. E. KING, *Acta Metall. Mater.* **39** (1991) 793.
8. K. LI, X.-D. JIN, B.-D. YAN and P.-X. LI, *Composites* **23** (1992) 54.
9. J. J. MASON and R. O. RITCHIE, *Mater. Sci. Eng.* **A231** (1997) 170.
10. M. LEVIN and B. KARLSSON, *Mater. Sci. Tech.* **7** (1991) 596.
11. S. KUMAI, K. YOSHIDA, Y. HIGO and S. NUNOMURA, *Int. J. Fatigue* **14** (1992) 105.
12. J. K. SHANG, W. YU and R. O. RITCHIE, *Mater. Sci. Eng.* **A102** (1988) 181.
13. X. LI and H. MISAWA, *Trans. Japan Soc. Mech. Engers.* **61** (1995) 251.

Received 18 October 2000
and accepted 22 June 2001